BUFFER LAYERS FOR NARROW BANDGAP A-SIGE SOLAR CELLS

X. B. LIAO, J. WALKER and X. DENG
Department of Physics and Astronomy, University of Toledo, Toledo, OH 43606

ABSTRACT

In high efficiency narrow bandgap (NBG) a-SiGe solar cells, thin buffer layers of unalloyed hydrogenated amorphous silicon (a-Si) are usually used at the interfaces between the a-SiGe intrinsic layer and the doped layers. We investigated the effect of inserting additional a-SiGe interface layers between these a-Si buffer layers and the a-SiGe absorber layer. We found that such additional interface layers increase solar cell V_{oc} and FF sizably, most likely due to the reduction or elimination of the abrupt bandgap discontinuity between the a-SiGe absorber layer and the a-Si buffer layers. With these improved narrow bandgap solar cells incorporated into the fabrication of triple-junction a-Si based solar cells, we obtained triple cells with initial efficiency of 10.6%.

INTRODUCTION

Narrow bandgap a-SiGe materials and solar cell devices have been studied extensively for their use in the spectrum splitting, multiple-junction a-Si based solar cells [1-3]. To achieve high conversion efficiency solar cells, an a-SiGe absorber layer is usually sandwiched between two thin a-Si buffer layers which are in direct contact with the p- and n- doped layers [3,4]. These a-Si buffer layers were found to enhance the performance of a-SiGe solar cells. However, even with these a-Si buffer layers, there are still abrupt discontinuity in the bandgap at the interfaces between these buffer layers and the a-SiGe absorber layer. In this paper, we report our study on the insertion of additional a-SiGe interface layers (with less Ge compared with the absorber) which reduces the bandgap offset.

EXPERIMENTAL DETAILS

The a-SiGe and a-Si materials used in this study were deposited using a ultra high vacuum plasma enhanced chemical vapor deposition (PECVD) system at the University of Toledo (UT). The intrinsic and doped layers were deposited in separated chambers of this multi-chamber, load-locked deposition system, having a base vacuum of 2×10^{-8} Torr. A gas mixture of GeH_4, Si_2H_6 and H_2 were used for the a-SiGe deposition and Si_2H_6 and H_2 for a-Si deposition. The deposition conditions include a substrate temperature range of 300-400 ^oC, a chamber pressure of 0.5-0.6 Torr and an rf power of 2.5-3.0 W for the a-SiGe and a-Si layer depositions. Different GeH_4 to Si_2H_6 ratios were used to achieve different bandgaps for a-SiGe material. Graded bandgaps for the a-SiGe absorber layer and the a-SiGe buffer layers were achieved by adjusting GeH_4 flows during growth. The GeH_4/Si_2H_6 gas flow ratio for the a-SiGe absorber layers studied here was 0.88. All of the intrinsic absorber and buffer layers were deposited in a deposition chamber designated for intrinsic layer growth.

Boron doped microcrystalline silicon (μc-Si) p-layer and phosphorus doped a-Si n-layer were deposited in another chamber designated for the growth of doped layers. The device structure used in this study v.as: SS/Ag/ZnO/n(a-Si)/b(a-Si)/i(NBG a-SiGe)/b(a-Si)/p(μc-Si)/ITO for the standard device and SS/Ag/ZnO/n(a-Si)/b(a-Si)/b(a-SiGe)/i(NBG a-SiGe)/b(a-SiGe)/b(a-

Mat. Res. Soc. Symp. Proc. Vol. 557 © 1999 Materials Research Society

Si)/p(μc-Si)/ITO for the new devices under study, where SS is stainless steel, Ag/ZnO is back-reflector, b(a-Si) and b(a-SiGe) are thin a-Si and a-SiGe buffer and interface layers, respectively. The ITO layer, serving as the top electrode and anti-reflection coating, was deposited using a rf sputtering process. Many of the I-V measurements were done using 0.05-cm^2 device without metal grids. Quantum efficiency (QE) measurements were used to measure spectral response and to obtain short circuit current (J_{QE}) by integrating the QE value over AM1.5 Global spectrum.

RESULTS AND DISCUSSIONS

Figure 1 shows the band structure of the various devices used in this study. Fig. 1a is a schematic of the structure for standard a-SiGe devices, showing two a-Si buffer layers on both sides of a-SiGe absorber layer. Fig. 1b and 1c show the schematics of the device structures with the additionally inserted a-SiGe interface layers having a fixed Ge content (Fig. 1b) and with interface layers having a graded bandgap (Fig.1c).

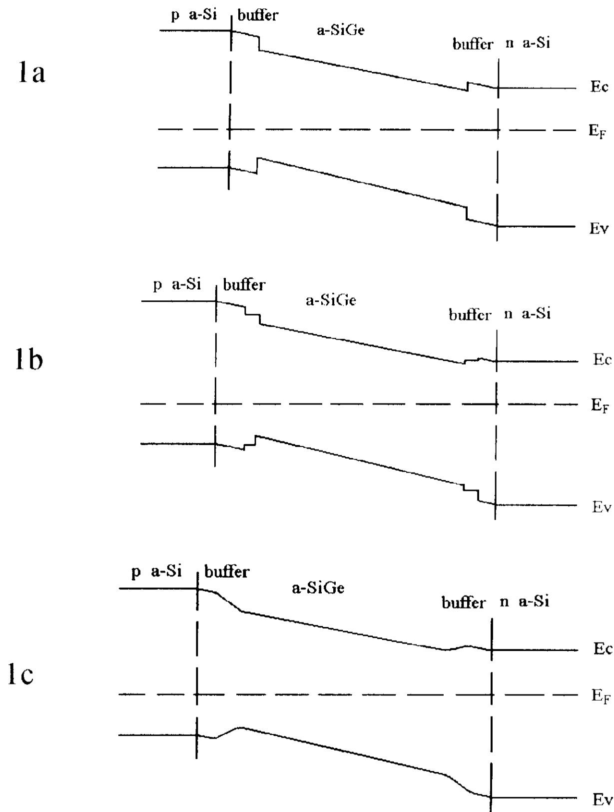

Fig.1a, 1b and 1c Schematic energy band diagram of a-SiGe solar cells with different interfacial buffer layers under the thermal equilibrium condition.

Table 1 lists the photovoltaic parameters of the open circuit voltage V_{oc}, short circuit current density J_{sc}, fill factor FF and the maximum power output P_{max} of a-SiGe solar cells with different interfacial buffers. GD180 is a standard a-SiGe device (Fig.1a) and GD202 contains a-SiGe buffer layers with a fixed Ge content inserted between the a-Si buffers and a-SiGe i-layer at both the n- and p-interfaces (See Fig.1b), while GD203 and GD209 have Ge-content graded buffer layers at both interfaces (See Fig.1c). It is clearly seen that the V_{oc} and FF have been increased due to the introduction of the additional a-SiGe interfacial layers and the improvements are approximately in the range of 2-5% for V_{oc} and 5-10% for FF. The V_{oc} and FF enhancement was higher for graded buffer layers. For this reason, the J-V characteristics of GD180 and GD209 are compared in Fig.2, and the results of these two devices are discussed further in the following.

Figure 3 shows the QE curves for a-SiGe cells without (GD180) and with (GD203 and GD209) bandgap graded interfacial layers. The spectral responses of these devices are approximately the same in the red region. The small variation in the red could also be due to the variation in the back-reflector. The difference in the blue region of the QE curve is mostly resulted from the variation in the transmission of ITO films.

Table 1 Photovoltaic parameters of solar cells with different buffer layers

Samples	V_{oc} (V)	J_{sc} (mA/cm^2)	FF	P_{max} (mW/cm^2)
GD180 Standard	0.647	23.5	0.506	7.7
GD202 w/ a-SiGe buffer	0.662	21.6	0.534	7.6
GD203 w/ graded a-SiGe buffer	0.680	23.4	0.536	8.5
GD209 w/ graded a-SiGe buffer	0.675	24.3	0.559	9.2

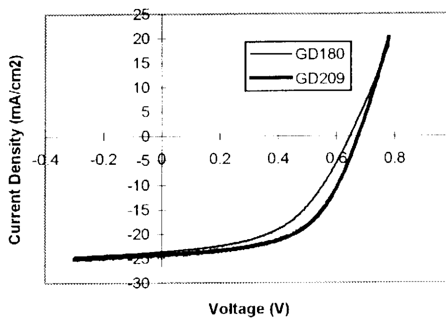

Fig.2 Illuminated J-V characteristics of GD180 and GD209 samples

Since small ITO contacts (0.05 cm^2) were used as the top electrodes, there might be some uncertainty in the active areas of the devices. Therefore, the J_{sc} values listed in Table 1 might not be highly precise. We used the current density values, J_{QE}, obtained by integrating the quantum efficiency curves over AM1.5 Global spectrum, as an independent check of the short circuit current values. Although the accuracy of absolute J_{QE} values from the QE measurements depend on the accuracy of the calibration of QE measurements, J_{QE} values obtained in this way are much more reproducible and precise than the J_{sc} values from the I-V measurements. The obtained J_{QE} and the relative P_{max} calculated from these J_{QE} values are summarized in Table 2. From this table, we find that the short circuit currents of standard a-SiGe sample (GD180) and the a-SiGe samples with graded buffer layers (GD203 and GD209) are approximately the same within the experimental variation. The enhancement in V_{oc} and FF result in a net increase in device P_{max}.

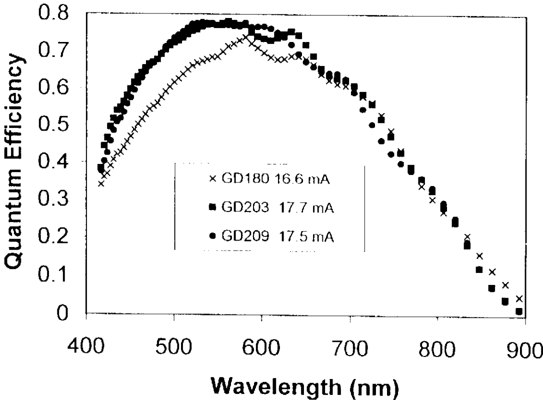

Fig.3 Quantum efficiency curves of a-SiGe solar cells. GD180 is standard solar cell, while GD203 and GD209 are cells with bandgap graded a-SiGe buffers.

Table 2 a-SiGe solar cell device performance

Sample	J_{QE} (mA/cm^2)	QE @800nm	V_{oc} (V)	FF	Relative P_{max} (mW/cm^2)
GD180	16.6	0.288	0.647	0.51	5.5
GD203	17.7	0.305	0.680	0.54	6.5
GD209	17.5	0.315	0.675	0.56	6.6

The influences on the performances of the solar cells from the recombination processes taking place at both interfaces between the intrinsic a-SiGe layer and doped layers could also be observed from the ideality factor (n) of the p-i-n devices. The improved J-V performance in the cells with bandgap graded a-SiGe interfacial layers are reflected also in the improvement of the ideality factor and the reduction in the reverse saturation current density (J_o) of these devices.

It is well known that the J-V characteristics of p-i-n a-Si solar cells under illumination can be approximately described by using transport equation of an ideal pn junction [5]:

$$J_{ph} = J_o [\exp(q(V - J_{ph}R_s) / nkT) - 1] - J_{sc} \quad (1)$$

where n is the ideality factor of the device under illumination, J_{ph} represents the photocurrent density, ($V - J_{ph}R_s$), in which J_{ph} could have negative value, represents the voltage at the junction of an ideal diode. The effect of the equivalent series resistance R_s is included in the equation, while the equivalent shunt resistance R_{sh} is not taken into account. In order to obtain n factor directly from experimental measurement, one could use the dependence of V_{oc} on J_{sc} under varying light intensities,

$$V_{oc} = (nkT/q)(\ln(J_{sc}/J_o + 1) \quad (2)$$

where the effect of R_s is avoided, hence n factor can be determined from the slope of the V_{oc} versus $\ln(J_{sc})$. Figure 4 shows the experimental data of J_{sc} (V_{oc}) measured under various light intensities for samples GD180, with the standard structure of a-SiGe bottom cell, and GD209, with a graded a-SiGe buffer layer at both interfaces. It is seen that there is a nearly linear relationship between $\ln(J_{sc})$ and V_{oc} with R-squared values of 0.9975 and 0.9998 for the two samples studied, consistent with the expectation of Eq. (2). From the slopes of these two lines we deduced the quality factor n to be 2.02 and 1.77, for the samples without (GD180) and with (GD209) graded a-SiGe interfacial layers at the p-i and i-n junction between the a-Si buffer layer and a-SiGe intrinsic layer, respectively. The reverse saturation current density, obtained from these fittings, were 8.3×10^{-8} A/cm^2 and 7.2×10^{-9} A/cm^2 for GD180 and GD209, respectively. The reductions in the n and J_o values indicate an improvement in the pn junction quality and a decrease in the recombination rate of extra minority carriers, as a result of these additional interfacial layers.

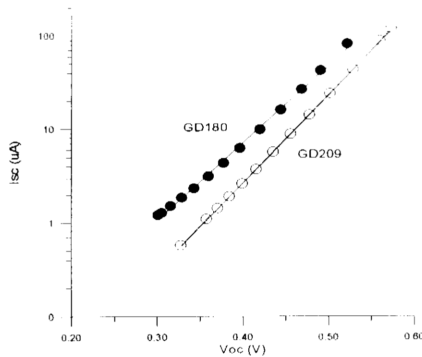

Fig.4 J_{sc} versus V_{oc} under various light intensity for samples GD180 (solid circle) and GD209 (open circle)

We incorporated the improved bottom cell into triple-junction a-Si based solar cells as the bottom cell. Figure 5 is a J-V curve for such a triple-junction solar cell measured at Energy

Conversion Devices, Inc. (ECD) under a solar simulator light, showing a 10.6% initial efficiency. Figure 6 is the QE curve for the triple-cell measured at ECD, showing a high integrated-total current of 23.6 mA/cm^2.

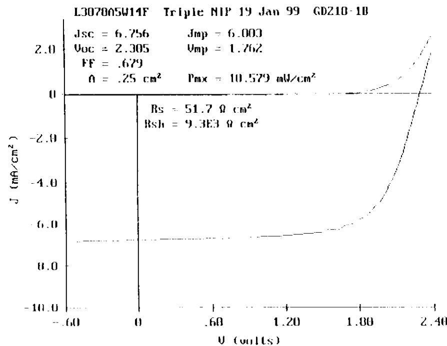

Fig. 5 J-V curve of a triple-junction solar cell incorporating the improved a-SiGe devices, showing an initial efficiency of 10.6%.

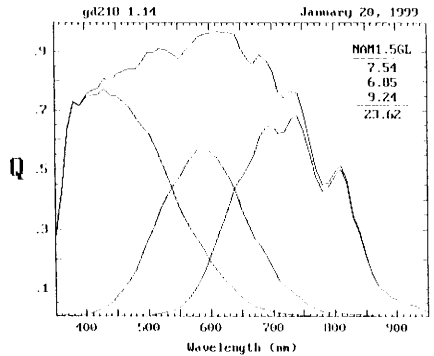

Fig. 6 QE curves of a triple cell incorporating the improved a-SiGe devices, showing an integrated J_{QE} of 23.6 mA/cm^2.

SUMMARY

We explored the effect of additional a-SiGe interface layers between narrow bandgap a-SiGe absorber layer and the a-Si buffer layers. The reduction and elimination in the bandgap offset at these interfaces result in sizable increases in device V_{oc} and FF, although the J_{sc} was somewhat unchanged. Incorporating NBG solar cells having such bandgap graded interface layers as the bottom cells, we fabricated triple-junction solar cells with 10.6% initial efficiency.

ACKNOWLEDGMENTS

We would like to thank Drs Al Compaan, Sijin Han, Pratima Agarwal, and Mr. Henry Povolny at UT, and Dr. Scott Jones and Mr. Tongyu Liu at ECD for discussions and help. This work was funded by NREL under the Thin Film Partnership Program (Subcontract No. ZAF-8-17619-14).

REFERENCES

1. See. Review by Y.S. Tsuo and W. Luft, Appl. Phys. Comm, **10**, 71 (1990) and references there in.
2. S. Guha, J.S. Payson, S.C. Agarwal and S.R. Ovshinsky, J. Non-Cryst. Solids 97-98, 1455 (1988).
3. J. Yang, R. Ross, T. Glatfelter, R. Mohr and S. Guha, MRS Poc. 149, 435 (1989).
4. X. Deng, "Development of High, Stable-efficiency Triple-junction a-Si Alloy Solar Cells", *Phase I Annual Subcontract Report*, July 18, 1994-July 17, 1995, prepared under Subcontract No. ZAN-4-13318-11. (February 1996). NREL/TP-411-20687. Available NTIS: Order No. DE9696000530.
5. S.M. Sze, Physics of Semiconductor Devices, 2nd Edition, John Wiley & Sons, New York, 1981.